
This is an electronic reprint of the original article.
This reprint may differ from the original in pagination and typographic detail.

Niemelä, Laura R.K.; Koskela, Essi V.; Frey, Alexander D.

Modification of the endoplasmic reticulum morphology enables improved recombinant antibody expression in *Saccharomyces cerevisiae*

Published in:
Journal of Biotechnology

DOI:
[10.1016/j.jbiotec.2024.03.009](https://doi.org/10.1016/j.jbiotec.2024.03.009)

Published: 20/05/2024

Document Version
Publisher's PDF, also known as Version of record

Published under the following license:
CC BY

Please cite the original version:
Niemelä, L. R. K., Koskela, E. V., & Frey, A. D. (2024). Modification of the endoplasmic reticulum morphology enables improved recombinant antibody expression in *Saccharomyces cerevisiae*. *Journal of Biotechnology*, 387, 1-11. <https://doi.org/10.1016/j.jbiotec.2024.03.009>

This material is protected by copyright and other intellectual property rights, and duplication or sale of all or part of any of the repository collections is not permitted, except that material may be duplicated by you for your research use or educational purposes in electronic or print form. You must obtain permission for any other use. Electronic or print copies may not be offered, whether for sale or otherwise to anyone who is not an authorised user.



Modification of the endoplasmic reticulum morphology enables improved recombinant antibody expression in *Saccharomyces cerevisiae*

Laura R.K. Niemelä, Essi V. Koskela, Alexander D. Frey*

Aalto University, Department of Bioproducts and Biosystems, Espoo, Finland

ARTICLE INFO

Keywords:

Saccharomyces cerevisiae
Endoplasmic reticulum
Reticulon
Recombinant protein expression

ABSTRACT

The yeast *Saccharomyces cerevisiae* is a versatile cell factory used for manufacturing of a wide range of products, among them recombinant proteins. Protein folding is one of the rate-limiting processes and this shortcoming is often overcome by the expression of folding catalysts and chaperones in the endoplasmic reticulum (ER). In this work, we aimed to establish the impact of ER structure on cellular productivity. The reticulon proteins Rtn1p and Rtn2p, and Yop1p are membrane curvature inducing proteins that define the morphology of the ER and depletion of these proteins creates yeast cells with a higher ER sheet-to-tubule ratio. We created yeast strains with different combinations of deletions of Rtn1p, Rtn2p, and Yop1p coding genes in cells with a normal or expanded ER lumen. We identified strains that reached up to 2.2-fold higher antibody titres compared to the control strain. The expanded ER membrane reached by deletion of the lipid biosynthesis repressor *OPI1* was essential for the increased productivity. The improved specific productivity was accompanied by an up to 2-fold enlarged ER surface area and a 1.5-fold increased cross-sectional cell area. Furthermore, the strains with enlarged ER displayed an attenuated unfolded protein response. These results underline the impact that ER structures have on productivity and support the notion that reprogramming subcellular structures belongs into the toolbox of synthetic biology.

1. Introduction

Intensification of endogenous metabolic activities and the endowment of cells with heterologous metabolic pathways is a cornerstone of biotechnology and enables production of a large variety of molecules. Similarly, rate limiting steps in protein production have been optimized and missing processing steps have been introduced to increase productivity and protein quality (Davy et al., 2017). In contrast, little attention has been given to investigate the impact of the structural context of cells on productivity. Recently, compartmentalization as a general strategy and the utilization of organelles as reaction sites for heterologous enzymes in particular have been recognized as important tool in the cell engineering repertoire (Hammer and Avalos, 2017). However, the potential of targeted modification of organelle size and morphology with a view towards improved cellular productivity has remained largely unexplored.

Comprehensive molecular level understanding of the biogenesis of the endoplasmic reticulum (ER) is available (Chen et al., 2012; Voeltz et al., 2006; West et al., 2011). Harnessing this knowledge, it was

observed that by genetically expanding the ER membrane heterologous protein production could be improved. Membrane expansion was controlled at two distinct levels, a the level of transcriptional control or of individual enzymatic activities (de Ruijter et al., 2016b; Guerfal et al., 2013; Koskela et al., 2017). The *OPI1* gene encodes the transcription repressor, which controls the activity of the heterodimeric Ino2p/Ino4p-complex transcription activator. The removal of *OPI1* gene encoding a transcription repressor resulted in constitutively active Ino2p/Ino4p transcription activator complex and resulted in a deregulated phospholipid biosynthesis and a 1.5-fold expansion of the yeast ER membrane (Schuck et al., 2009a). The benefits of the *OPI1* deletion to increase protein production were two-fold: first, an increased ER volume was obtained, secondly, the enlarged ER volume could be populated with folding catalysts and chaperones boosting the productivity (de Ruijter et al., 2016b; Koskela et al., 2017). Similarly, proliferation of ER membranes by inactivation of *PAH1* improved the accumulation of a recombinant membrane-localized receptor in the yeast *Yarrowia lipolytica*. The *PAH1* deletion disrupted synthesis of storage lipids by blocking the conversion of phosphatidic acid into diacylglycerol,

* Correspondence to: Bioproducts and Biosystems, Aalto University, Kemistintie 1, Espoo 02150, Finland.

E-mail address: alexander.frey@aalto.fi (A.D. Frey).

<https://doi.org/10.1016/j.jbiotec.2024.03.009>

Received 21 October 2023; Received in revised form 23 March 2024; Accepted 24 March 2024

Available online 28 March 2024

0168-1656/© 2024 The Author(s). Published by Elsevier B.V. This is an open access article under the CC BY license (<http://creativecommons.org/licenses/by/4.0/>).

diverting phosphatidic acid to phospholipid biosynthesis instead and resulting in proliferation of ER and nuclear membranes (Guerfal et al., 2013).

Besides the ER membrane area, also its morphology is genetically controlled. Morphologically, the ER can be divided into three distinct domains: the central cisternal ER around the nucleus, the plasma-membrane associated ER, and the tubular ER, which extends into the cytosol from the two other structures (West et al., 2011). Importantly, these morphologies correlate with distinct ER functions, sheet-like ER structures are the sites for protein folding, while the tubular ER is the primary site for lipid biosynthesis. The presence of curvature inducing reticulon/REEP proteins (Rtn1p, Rtn2p and Yop1p) is responsible for forming ER tubules and depleting ER membrane curvature inducing proteins increases ER sheet-to-tubule ratio (Voeltz et al., 2006). Reticulons are not only found in tubular ER, but Rtn1p is also found in the high curvature areas of the ER sheets and *RTN1* expression has been shown to affect the ER sheet to tubule ratio (Shibata et al., 2010). Branching inducing proteins (Sey1p) supported by the protein Lnp1 are responsible for forming the highly interconnected tubular ER network (Chen et al., 2012). The understanding on the formation of the sheet-like ER structures is still incomplete. Among the candidates to stabilize the flat surfaces of the ER cisternae are polyribosomes associated with translocation machinery. In yeasts, the ratio between membrane surface area and the abundance of the Rtn1 Rtn2 and Yop1p appears to be the decisive factor determining the morphology of the ER (Westrate et al., 2015).

In this research we investigated the secretion capacity of *S. cerevisiae* when modifying the ER morphology for an increased size and a higher ratio of ER sheets compared to tubules. We created a strain set lacking the membrane curvature inducing genes (*RTN1*, *RTN2*, *YOP1*) and the *OPII* gene in different combinations and investigated the secretion capacity of these strains by expressing different mammalian proteins. The increased productivity observed in the best performing strains was accompanied by an enlarged ER surface area and an attenuated unfolded protein response (UPR).

2. Methods

2.1. Generation of yeast strains

All strains used in this study were based on the wild-type laboratory strains W303 α and SS328 (Supplementary Table S1). The strains YEK018 and YEK019 served as chassis strains to create the two deletion strain families used in the screening. These strains contain a genomic copy of the antibody expression construct under control of the *GAL1* promoter and have been described elsewhere (de Ruijter et al., 2016b). The strain YEK019 lacks in addition the complete *OPII* gene. The deletion strains without the genomic copy of the antibody expression construct were derived from W303 α and SS328.

All gene deletions were created by transforming PCR generated knock-out cassettes comprising a dominant selection marker flanked by loxP sites encoded on plasmids pUG6 or pUG74 and gene specific targeting sequences using lithium acetate method (Gietz and Schiestl, 2007; Hegemann and Heick, 2011). The oligonucleotides used to generate knock-out cassettes and confirm deletions are listed in Supplementary Table S2. Deletions were confirmed with PCR using oligonucleotide pairs comprising of an oligonucleotide binding upstream of the deleted gene (EK007, EK082, EK083 and EK084) and one within the deletion cassette (OJR96). Selection markers were removed using Cre-recombinase expressed from plasmid pSH47 following published protocols (Hegemann and Heick, 2011).

The UPR reporter strains YLN017, YLN018, and YLN019, were created by introducing the linearized plasmid pDEP17 comprising four UPR-response element sequences upstream of a minimal promoter and the NdegY-GFP sequence into the *TRP1* locus (Pincus et al., 2010) and these strains complemented the set of previously generated strains

YMR24, YJR129, and YEK063 (de Ruijter et al., 2016a, 2016b).

All plasmids used in this study are listed in Supplementary Table S3. In the experiments the empty plasmids pEK7 and pEK17 were used in control strains to complement *LEU2* and *URA3* auxotrophies. These plasmids correspond to circularized, promoter less versions of pRS415 and pRS426 vectors, respectively.

A codon optimized DNA fragment encoding a synthetic nanobody human IgG heavy chain antibody (Nb-HCAB) from Eurofins and cloned into *SpeI XhoI* sites of pRS416-GAL1 vector generating plasmid pLK1. The coding sequence of the Nb-HCAB contains the signal sequence of the *OST1* gene (amino acids 1–23) and the nanobody coding sequence from (Walter et al., 2022) that is fused to the linker region and the CH₂ and CH₃ domains of a human heavy chain. Assembly of the fusion was designed essentially as described for other antibody fusion constructs (Parsaie Nasab et al., 2013).

Plasmid pAX423 contains the mating factor alpha pre-pro sequence (Mat α) and the coding sequence of the mature human secreted alkaline phosphatase (SEAP, amino acids 23–506) with a C-terminal His-tag. PCR amplified Mat α (oligonucleotides OAF236 and OAF237) and SEAP (oligonucleotides OAF254 and OAF255) were digested with *BamHI/NheI* and *NheI/HindIII*, respectively and inserted into plasmid pSL1180. The Mat-SEAP fusion was excised and inserted into *BamHI/HindIII* sites of pRS426-GAL1. Plasmid pAX37 contains the PCR amplified yeast *DGK1* gene (oligonucleotides OAF98 and OAF99) inserted into *SpeI XhoI* sites of pRS426-GAL1 placing it under the control of the *GAL1* promoter.

2.2. Yeast cultures

Yeast strains without plasmids were routinely grown in YPD or complete synthetic medium (0.67% yeast nitrogen base without amino acids, 1.7 g/L amino acid, and a carbon source). Yeast strains containing plasmids were grown in synthetic drop-out medium lacking uracil (0.67% yeast nitrogen base without amino acids, 1.7 g/L amino acid mix lacking uracil, and a carbon source).

Expression tests were conducted in 24-well deep well plates in 4 ml of medium. For expression of antibodies, a medium containing two-fold concentrated synthetic casamino acid amino acid mixture (2x SCAA) as described (Shusta et al., 1998), 0.5% raffinose, 50 mM sodium phosphate, pH 6.5, 0.1 μ g/ml BSA, 12.5 mM arginine and 0.0025% Tween-20 was used. Precultures were used to inoculate fresh 2x SCAA medium to a starting OD₆₀₀ of 0.2. Antibody expression was induced with 0.5% galactose six hours after inoculation and expression was continued for up to 48 hours at 28 °C and 220 rpm.

To produce secreted alkaline phosphatase (SEAP), strains were grown at 30 °C and 230 rpm. SEAP expression was induced with 4% galactose after 5.5 hours. Expression was continued for 24 hours. To produce yeast acid phosphatase, strains were grown at 30 °C and 220 rpm. Yeast acid phosphatase expression was induced with 2% galactose and continued for 16 hours.

2.3. Small-scale cultivations

Growth curves of the deletion and control strains were recorded from cultivations conducted in round-bottom 96-well microtiter plates. Precultures were grown in complete synthetic medium for 24 hours at 30 °C and 220 rpm. Precultures were used to inoculate 100 μ l/well of complete synthetic medium containing either 0.5% glucose or galactose to an OD₆₀₀ of 0.1. Growth curves were recorded at 28 °C for 48 hours.

Growth of UPR reporter strains was conducted in round-bottom 96-well microtiter plates. Precultures were grown in SD medium for 24 hours at 30 °C and 220 rpm. Precultures were used to inoculate 100 μ l/well of 2x SCAA medium to an OD₆₀₀ of 0.1. Strains were either induced with 0.5% galactose or repressed with equal amount of glucose six hours after inoculation and grown at 28 °C for 48 hours.

96-well microtiter plates were incubated using continuous double orbital shaking (807 rpm, 1 mm). Cell growth (optical cell density at

595 nm) and GFP signal (excitation 485 nm, emission 528 nm) were recorded at 15-minute time intervals with a Cytation 3 Microplate Spectrophotometer (BioTek, Winooski, USA).

2.4. Spotting assays

Spotting assays were performed as described (de Ruijter and Frey, 2015). Serial dilutions of deletion and control strains were plated on glucose (SD) or galactose (SGal) containing complete synthetic medium plates and incubated at 28 °C. The SD plates were incubated for 48 hours before imaging and the SGal were incubated for 72 hours before imaging.

2.5. Quantification of recombinant protein expression

Titers of different antibodies were determined from cleared culture supernatants that were adjusted to 1x PBT (135 mM NaCl, 2.5 mM KCl, 10 mM Na₂HPO₄, 1.75 mM KH₂PO₄ with 0.05% Tween-20) with an enzyme-linked immunosorbent assay (ELISA) as described (de Ruijter and Frey, 2015).

SEAP activity was determined from cleared culture supernatant samples. Endogenous alkaline phosphatase activity was inactivated by incubating samples for 30 min at 65 °C. The SEAP assay reaction buffer consisted of 100 mM Tris-HCl pH 9.5, 5 mM MgCl₂, 100 mM NaCl, and 0.2% Triton X. The substrate solution was composed of 20 mM para-nitrophenylphosphate (pNPP) in reaction buffer. The experiment was conducted in microtiter plate format with a Synergy H1 Microplate Spectrophotometer (BioTek, Winooski, USA). The reaction was started by adding 100 µl substrate to wells which contained 50 µl buffer and 50 µl sample. The blank consisted of 100 µl buffer and 100 µl substrate. Absorbance was read at a wavelength of 405 nm for 16 hours every 10 min at 37 °C and the endpoint activity was documented.

Secreted yeast acid phosphatase activities were determined from cleared culture supernatants by measuring the consumption of pNPP as described (Koskela et al., 2020).

2.6. Monitoring of *Kar2p* expression

Cell extracts were prepared as described in (Pirainen and Frey, 2020). Samples were resolved on 12.5% SDS-PAGE gels before immunoblotting. Immunoblotting and Ponceau S staining was conducted essentially as described. A rabbit polyclonal antibody (Kar2 (y-115), sc:33630, Santa Cruz Biotechnology, Inc.) was used for the detection of the Kar2 protein in 1:1'000 dilution with a secondary antibody (Anti-Rabbit IgG (whole molecule)-Peroxidase antibody produced in goat, Sigma-Aldrich A0545) in 1:50'000 dilution. Image Lab 5.1 Software was used for the analysis of the immunoblots.

2.7. ER staining

ER staining was performed essentially as described (Bao et al., 2018). Control and *DGK1* expressing strains were grown in SD-URA at 30 °C and 220 rpm. Precultures were grown overnight and used to inoculate expression cultures. *DGK1* expression was induced by the addition of 0.5% galactose. Cells were harvested when OD₆₀₀ reached 1.0. Deletion and control strains were grown according to the same protocol but replacing SD-URA with YPD medium.

1 OD₆₀₀ unit of cells was harvested by centrifugation and cells were washed twice with PBS and once with Hank's balanced salt solution (HBSS). Cells were resuspended in 1 ml HBSS and 5 µl of ER-Tracker™ Blue-White DPX. Samples were incubated for 30 min at 30 °C and washed with HBSS. Finally, the samples were resuspended in 1 ml HBSS and loaded to a black well plate. Fluorescence signals (excitation 374 nm, emission 551 nm) were recorded with a Synergy H1 Microplate Spectrophotometer (BioTek, Winooski, USA).

2.8. Microscopy

For microscopy precultures of the control and deletion strains were grown overnight in YPD medium at 30 °C and 220 rpm. Cultures were inoculated the next morning in YPD medium and grown until OD₆₀₀ 1.0 was reached. Cells were washed twice with PBS and resuspended in PBS for microscopy. Brightfield images were acquired using a Zeiss Axio Observer Z1/ 7 microscope with a 100×1.4 oil Plan-Apochromat objective and a 1.6x tube lens. Zen Zeiss software was used for image acquisition and analysis. Five to seven images were analyzed for each strain and images were acquired from different sections of one slide. The aim was to choose randomly 100 non-budding cells that resided in the same focal plane for analysis. The cell area at the mid sections of cells were quantified. For confocal laser scanning microscopy, the cells were stained with ER-Tracker™ Blue-White DPX as described before. The images were acquired using a 100x oil objective with a 1.5x tube lens. The imaging was done with 200 ms exposure time, at a 405 nm wavelength with 50% laser intensity, and using a 405 Xlight QuadLM.

2.9. Physicochemical properties of proteins

Secreted yeast and human proteins were identified from Uniprot database using the search terms “secreted” and “*Saccharomyces cerevisiae*” or “*Homo sapiens*”. Forty proteins were picked from the curated search results that excluded proteins that were misannotated, and their amino acid composition, isoelectric point (pI) and grand average of hydropathicity index (GRAVY) was calculated (Kyte and Doolittle, 1982).

2.10. Data processing

All numeric data was analyzed using GraphPad Prism 6 software package and is displayed as box plots depicting the range (minimum to maximum), quartiles and median of four to eight biological replicates. For image analysis between 72 and 107 cells were analyzed per strain. Ordinary one-way ANOVA followed by Tukey's multiple comparison test or paired t-test were applied.

3. Results

3.1. Modifications of the ER morphology and size can affect phenotype

It was earlier noticed that depleting ER membrane curvature inducing proteins increases ER sheet-to-tubule ratio and expands the sheets (Voeltz et al., 2006). Similarly, deleting the *OPI1* gene was observed to affect the size and shape of the ER, expansion preferably increasing the sheet structures, possibly due to the limiting amount of the reticulin proteins (Schuck et al., 2009a; Voeltz et al., 2006). Motivated by earlier work that revealed a positive correlation between ER expansion and productivity of secreted proteins, we were interested to investigate how the morphology of the ER affects the expression capacity of yeast for heterologous proteins (de Ruijter et al., 2016; Koskela et al., 2017).

To this end, we created strains with a galactose inducible antibody expression cassette which were lacking the ER membrane curvature inducing genes *RTN1*, *RTN2*, and *YOP1* alone or in different combinations. We created these deletions in the wild-type (referred to as Opi1⁺) and in the *OPI1* gene deletion background (referred to as Opi1⁻). First, we conducted spotting assays to test for any growth phenotype of the strains. All strains grew well in repressing conditions and no significant growth defects were visible (Fig. 1a). After incubating the strains for 72 hours in inducing conditions we observed that the *Δrtn1* strain and the triple deletion strain *Δyop1Δrtn1Δrtn2* did not form any colonies on the inducing SGal plates (Fig. 1a).

To further characterize the strains, we monitored their growth in a 96-well plate microtiter plate system. Generally, the strains with the

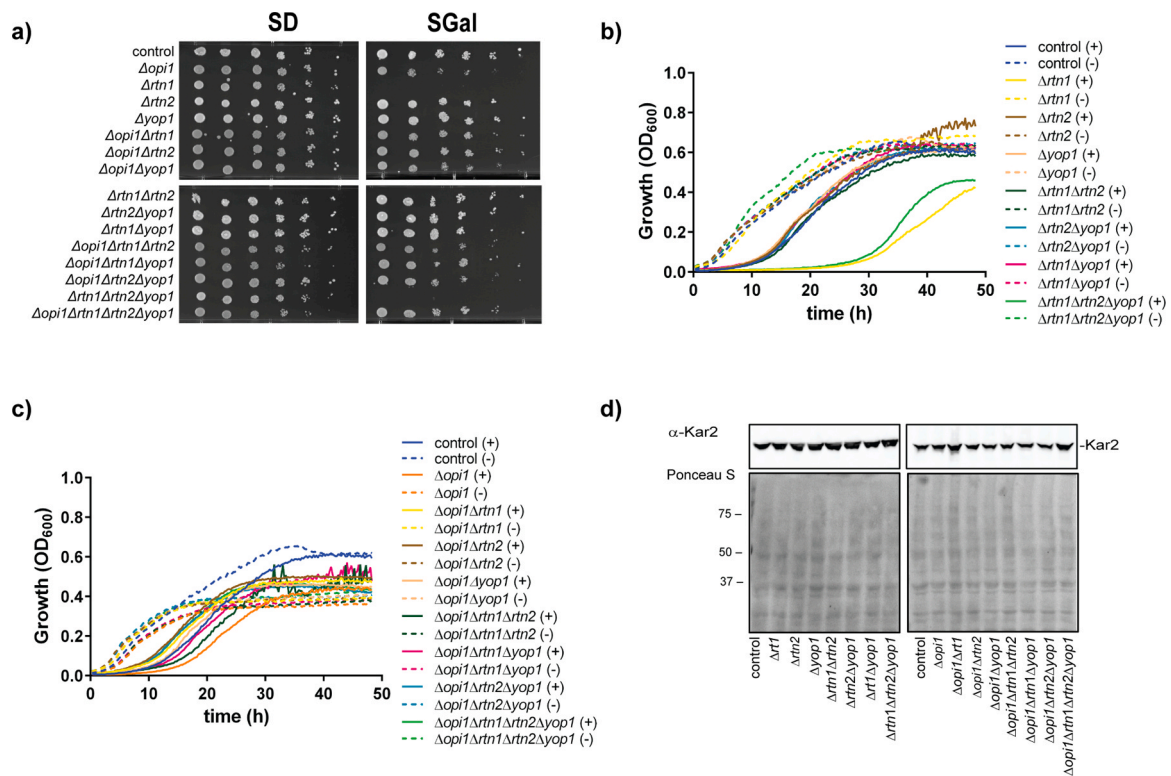


Fig. 1. Phenotypal characterization of yeast strains with engineered ER size and morphology. a) Growth phenotypes of the deletion and control strains on solid growth medium. Serial dilutions of strains harboring a galactose inducible antibody expression cassette were spotted on complete synthetic medium plates with either glucose (SD) or galactose (SGal). Plates were incubated at 28 °C for 2 days (SD) or 3 days (SGal). b) & c) Growth curves of deletion and control strains grown in 96-well microtiter plates. Cells were grown in synthetic medium containing either 0.5% galactose for inducing conditions (continuous lines, + sign after strain name) or 0.5% glucose for repressing conditions (dashed lines, - sign after strain name) at 28 °C for 48 h. Strains with $Opi1^+$ background are presented in panel (b) and strains with $Opi1^-$ background in (c). The strain YEK18 (control) is included in both panels. Growth curves represent averages from duplicate cultures. (d) Effects of ER manipulation on Kar2p levels. Cell extracts were prepared from strains grown in rich medium and analyzed for the expression of the ER protein Kar2p. Total protein was visualized using Ponceau S staining and used as loading control.

$Opi1^-$ background reached lower OD₆₀₀ values, irrespective whether induced or repressed (Fig. 1b, c). Under repressing conditions, there were no notable differences in the growth among the deletion strains with the $Opi1^+$ background (Fig. 1b). The strains of the $Opi1^-$ background, however, entered the stationary phase at lower OD₆₀₀ values and reached lower maximal cell densities compared to the control (Fig. 1c). Under these conditions, the final OD₆₀₀ values of the $\Delta opi1$ and the quadruple deletion strain were reduced to 59% and 68%, respectively, of the control.

When induced, the growth of strains with the $Opi1^+$ background did not differ considerably from the control (Fig. 1b, continuous lines). However, the $\Delta rtn1$ and the $\Delta yop1 \Delta rtn1 \Delta rtn2$ strains showed a substantially longer lag phase and reduced final cell density compared to the other deletion strains and the control strain (Fig. 1b). In induced conditions, the $\Delta opi1$ strain and the quadruple deletion strain reached final cell densities which were 73% of the cell density of the control strain. Also the $\Delta opi1$ strain, and the $\Delta opi1 \Delta rtn1 \Delta rtn2$ strain displayed longer lag phases than the other deletion strains with the $Opi1^-$ background and the control strain (Fig. 1c). Overall, the results obtained from the small-scale cultivations correlate well with the observations made from spotting assay showing a growth phenotype when antibody expression is induced.

To test if the modifications would influence ER function, we verified the expression of the ER protein Kar2p which is under control of the unfolded protein response (UPR) by immunoblotting (Travers et al., 2000). In short, Kar2p expression in the deletion strains in comparison to the control was not affected (Fig. 1d).

3.2. Modifications of the ER morphology and size increased productivity

Next, we screened all fifteen deletion strains and the control strain in 24-well deep well plate format for their antibody production capacity. We observed that the strains with the $Opi1^-$ background reached higher specific antibody titers compared to the strains with the $Opi1^+$ background (Fig. 2a, Supplementary Table S4). The specific IgG titer of the $\Delta opi1$ strain seemed 1.6-fold higher compared to the control strain, aligning with our earlier results (de Ruijter et al., 2016b). The strains $\Delta opi1 \Delta rtn2 \Delta yop1$, $\Delta opi1 \Delta rtn1 \Delta rtn2$ and $\Delta opi1 \Delta rtn1 \Delta rtn2 \Delta yop1$ reached more than 2-fold higher specific antibody titers compared to the control strain ($P < 0.05$). As observed in the small-scale cultivation experiments, final cell densities of strains with $Opi1^-$ background were lower (Fig. 2b). Furthermore, the two strains exhibiting poor growth in the previous cultivation tests displayed also very low expression levels and very strong growth phenotypes after 24 hours of growth, but they recovered to some extent after 48 hours (Supplementary Table S5). In addition, we analyzed the expression of Kar2 under antibody expressing conditions in relation to non-expressing conditions. Generally, the normalized signals of the investigated strains were on a similar level (Supplementary Fig. S1, Supplementary Table S6).

As modifications of the ER size and morphology had such strong effects on specific product yield, we concluded that one of the major bottlenecks of IgG secretion must be ER-related processes whether it being folding, translocation or exit from the ER. As a model of protein transit through the ER in *P. pastoris* suggested that the relative rate of secretion decreases with increasing complexity of the cargo protein (Love et al., 2012), we decided to express a less complex, but structurally related protein, a chimeric nanobody. The nanobody has a lower

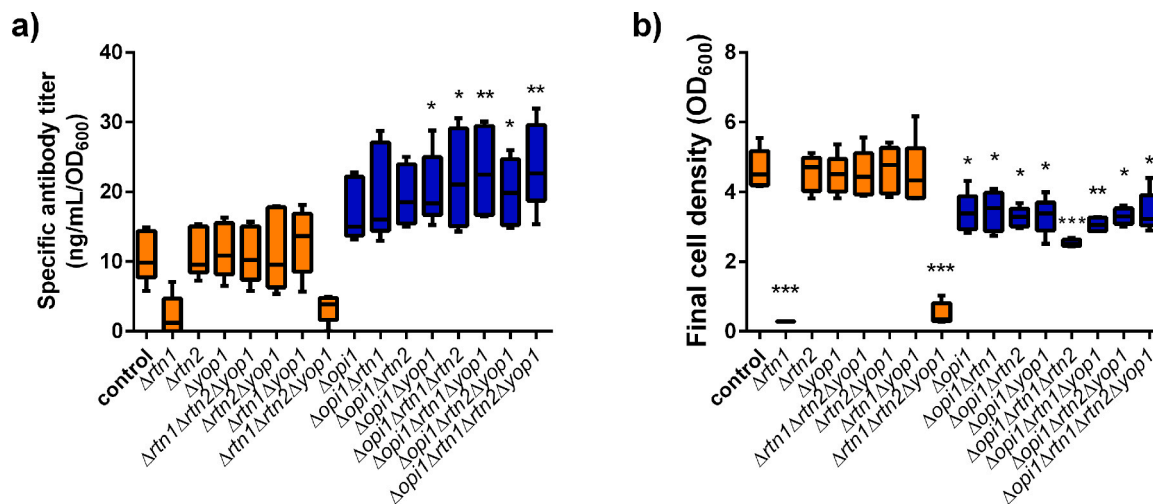


Fig. 2. Effects of ER size and morphology on full-size antibody expression. Deletion and control strains expressing a genomically encoded full-size antibody were cultivated in 24-well deep well plates. Specific antibody titers (a) and final cell densities (b) determined 24 hours after inducing protein expression with 0.5% galactose are depicted. Strains from Opi1⁺ and Opi1⁻ background are colored red and blue, respectively. The range, 10–90 percentile and median of five biological replicates, except for strains Δ opi1 Δ trn1 Δ trn2 and Δ opi1 Δ trn1 Δ yop1 for which the results of four biological replicates are displayed. P-values were calculated by pairwise comparison of deletion strains to the control strain. *: $P < 0.05$; **: $P < 0.01$; ***: $P < 0.001$.

molecular weight and the protein folding requires only dimerization of two identical subunits. Based on the obtained results, we selected four genotypes, all with Opi1⁻ background, and generated deletion strains in two different genetic strain backgrounds, W303 α and SS328 for comparison. We expressed the nanobody construct in these strain sets and observed that the specific titers for this construct seemed to be throughout all tested strains at least about 2-fold higher compared to the full-length antibody expression (Figs. 2a, 3a). All deletion strains derived from W303 α displayed an increased specific titer compared to the control after 24 hours with the best strains reaching approximately 1.3-fold higher levels ($P < 0.001$) (Fig. 3a, Supplementary Tables S7–S8). The positive effects of the deletions were also observed with the strains derived from SS328. Although, these strains reached lower final cell densities and antibody titers, the improvements in specific titers compared to the control were of similar magnitude as observed for the strains derived from W303 α (Supplementary Tables S7–S8).

Based on our current and previous works we were aware that the

effect of cell engineering on productivity is often specific for the target protein. Therefore, we also studied how useful the most interesting deletion strain would be in enhancing expression of other proteins in comparison to the control strain. Hence, endogenous AP and secreted alkaline phosphatase (SEAP) were expressed in the wild-type, and two deletion strains, Δ opi1 and Δ opi1 Δ trn1 Δ trn2 Δ yop1, which improved expression to different degrees over the control in our previous experiments. The specific yeast AP activity of the Δ opi1 and the Δ opi1 Δ trn1 Δ trn2 Δ yop1 strains were not statistically different from the control reaching about 0.9-fold and 1.1-fold, respectively, of the control strain (Fig. 4a, Supplementary Table S9). In contrast, the specific SEAP activity of the Δ opi1 and the Δ opi1 Δ trn1 Δ trn2 Δ yop1 strains appeared to be enhanced by 1.3-fold and 1.5-fold, respectively, compared to the wildtype control after 24 h of protein expression ($P > 0.05$) (Fig. 4c, Supplementary Table S10). The final OD₆₀₀ of the deletion strains were considerably lower compared to the corresponding wildtype control strains (Fig. 4b, d, Supplementary Table S9, S10).

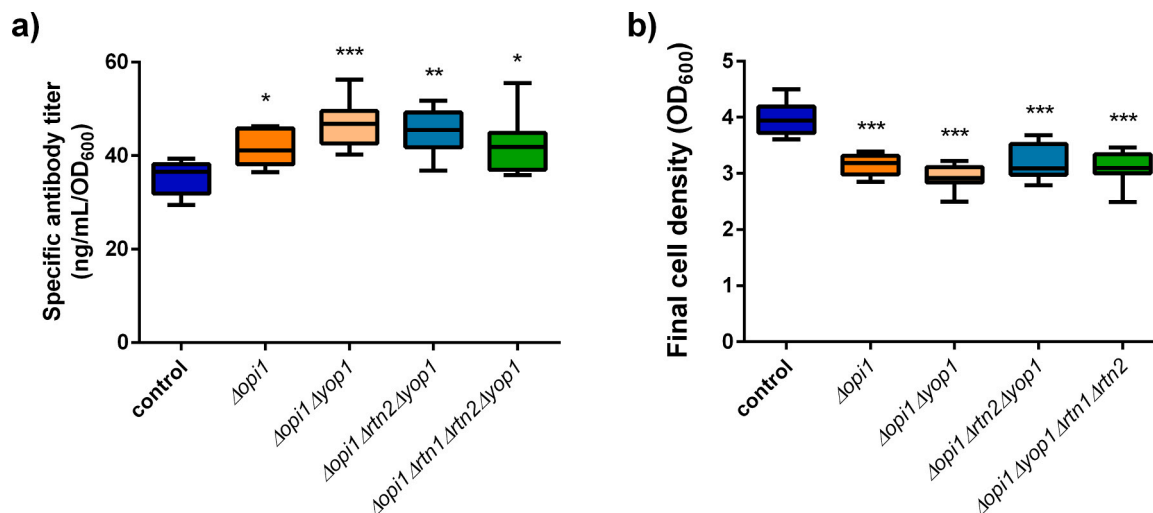


Fig. 3. Effects of ER size and morphology on expression of a nanobody. Selected deletion and control strains expressing a plasmid encoded nanobody were cultivated in 24-well deep well plates. Specific antibody titers of the secreted nanobody (a) and final cell densities (b) determined 24 hours after inducing protein expression with 0.5% galactose are depicted. The range, 10–90 percentile and median of eight biological replicates are displayed. P-values were calculated by pairwise comparison of deletion strains to the control strain. *: $P < 0.05$; **: $P < 0.01$; ***: $P < 0.001$.

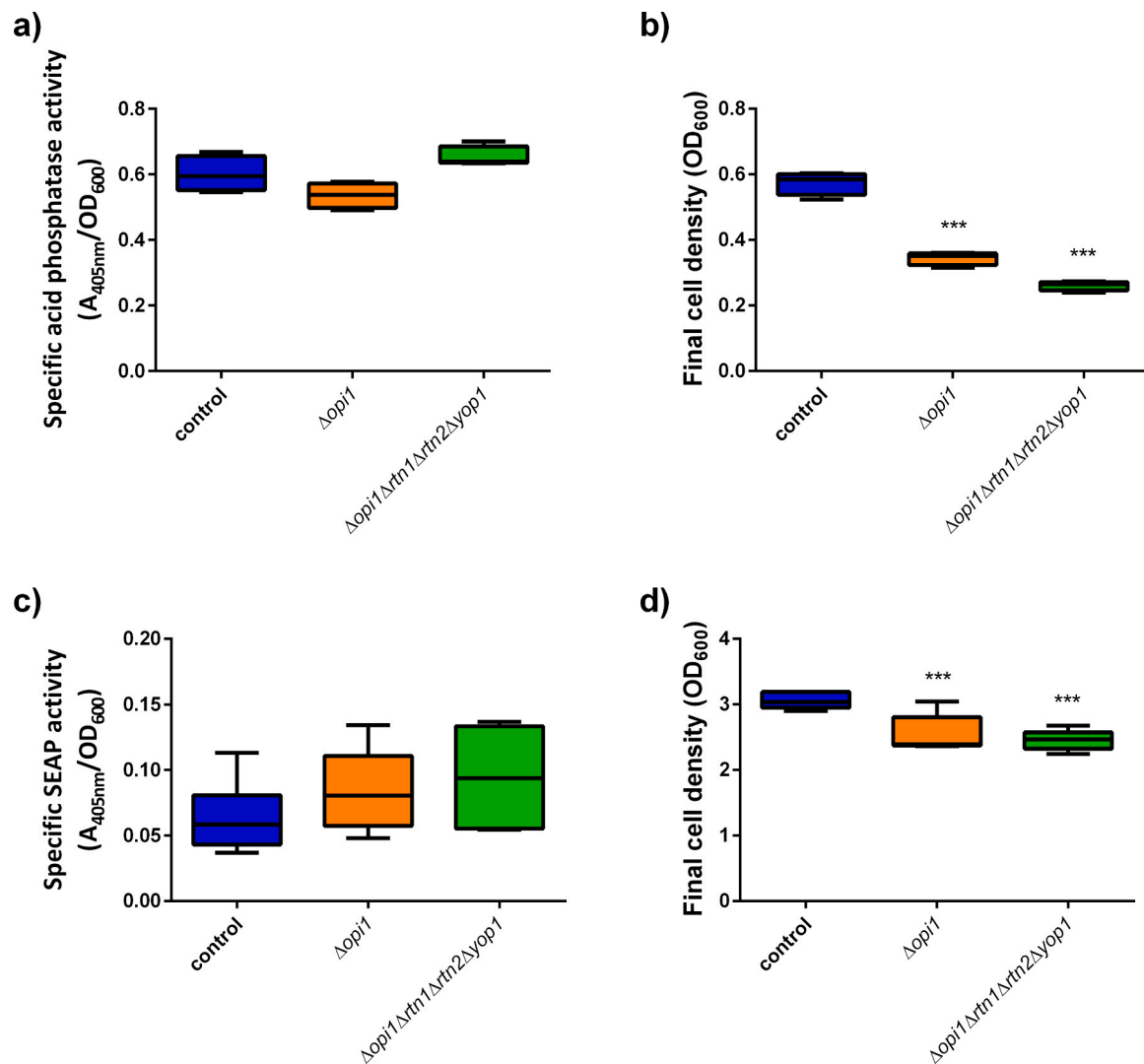


Fig. 4. Effects of ER size and morphology on expression of phosphatases. Selected deletion and control strains expressing either yeast acid phosphatase or secreted alkaline phosphatase (SEAP) were cultivated in 24-well deep well plates. Strains expressing yeast acid phosphatase were induced with 2% galactose and enzyme activity was determined 16 hours after induction. Strains expressing SEAP were induced with 4% galactose and enzyme activity was determined 24 hours after induction from heat inactivated culture supernatants. Specific secreted phosphatase activities (a & c) and final cell densities (b & d) of strains expressing yeast acid phosphatase (a & b) or secreted alkaline phosphatase (c & d) are shown. The range, 10–90 percentile and median of four to six biological replicates are shown. P-values were calculated by pairwise comparison of deletion strains to the control strain. *: $P < 0.05$; **: $P < 0.01$; ***: $P < 0.001$.

As all proteins of mammalian origin (antibody, nanobody and SEAP) were expressed to higher levels in the strains with the manipulated ER morphology, we randomly sampled forty secreted human and yeast proteins each and determined their amino acid composition and their hydrophobicity and isoelectric points (Fig. 5, see Supplementary Tables S11, S12). Our analysis showed significant changes in the content of Ala, Cys, Ile, Leu, Pro, Arg, Ser and Thr (Fig. 5a). Furthermore, we noticed that the average pI of the sampled yeast proteins is 5.23 and is significantly lower ($P < 0.01$) than the average pI of the mammalian proteins of 7.42 yielding more strongly charged proteins when present in the pH neutral environment of the ER. Furthermore, we determined the hydrophobicity of the sampled proteins; the grand average of hydropathicity index (GRAVY) was -0.341 for the sampled human proteins and -0.185 for the yeast proteins indicating that the human proteins are on average less polar than the yeast proteins ($P < 0.001$).

3.3. Deletion of membrane curvature inducing genes increased ER surface area

As the morphological effects of the deletion of curvature inducing

proteins had been well characterized in the past (Voeltz et al., 2006; West et al., 2011), we were interested in assessing the extent of ER membrane expansion. To this end, we used a fluorescence-based dye assay that enables to quantify the changes in the ER membrane surface area (Bao et al., 2018; Diwu et al., 2000). We first verified the assay by controlled overexpression of yeast *DGK1*. *DGK1* expression causes the expansion of the perinuclear ER membrane (Han et al., 2008). Our test showed that the ER membrane surface area increased by a factor of 3.0 upon expression of *DGK1* compared to the control cells (see Supplementary Fig. S2). To assess only the effects of the gene deletions in an isolated manner and exclude any interferences by the unfolded protein response (UPR) that could also induce ER expansion, we conducted these experiments without any overexpression. The $\Delta\text{opi1}\Delta\text{trn1}\Delta\text{trn2}\Delta\text{yop1}$ quadruple deletion strain showed the greatest ER expansion in comparison to the control strain (Fig. 6a). The normalized ER membrane surface area of the quadruple strain was 2-fold higher ($P < 0.01$) than that of the control strain suggesting a considerable ER expansion. The measured ER surface area for the Δopi1 and the $\Delta\text{opi1}\Delta\text{yop1}$ deletion strains seemed 1.2-fold higher than that of the control strain, while the $\Delta\text{opi1}\Delta\text{trn2}\Delta\text{yop1}$ triple deletion strain seemed

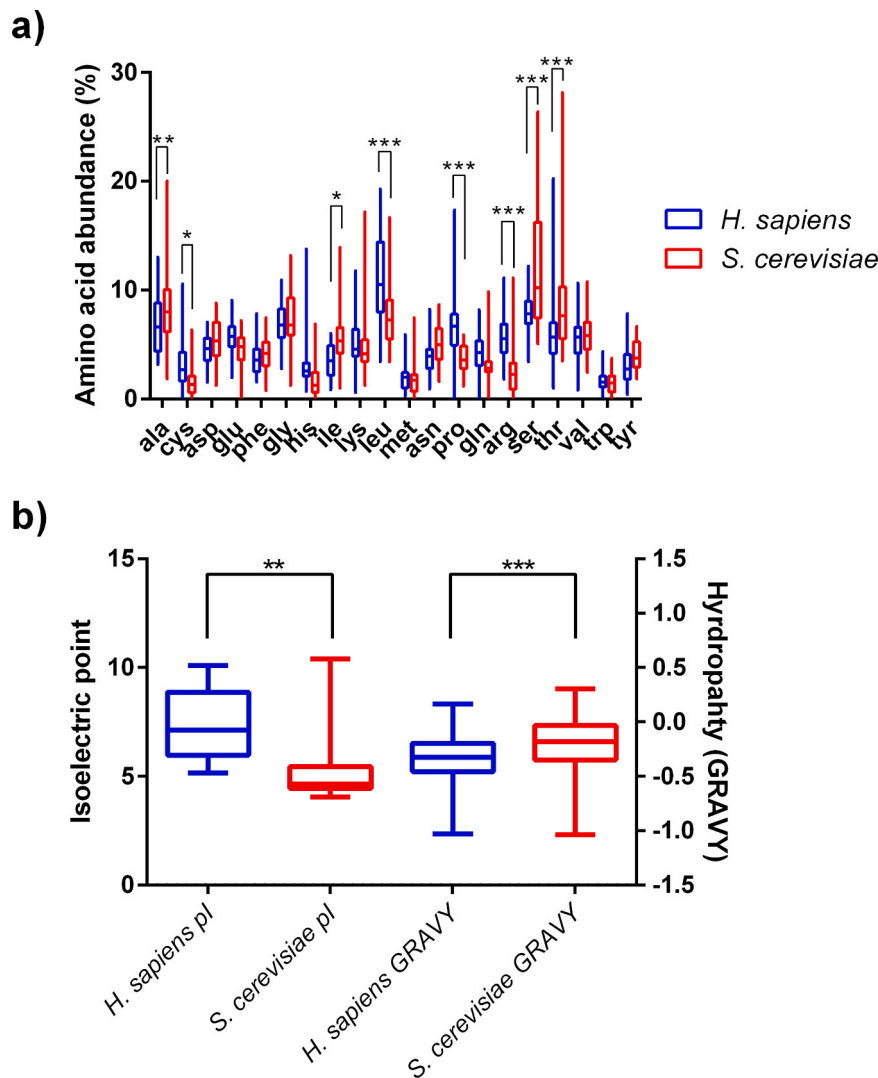


Fig. 5. Comparison of amino acid composition, isoelectric point (pI) and hydropathy of yeast and human proteins. Forty secreted human and yeast proteins picked from a shortlist generated by *uniprot* were analyzed for their amino acid composition (a) and the resulting isoelectric point and hydropathy (b). The range, 10–90 percentile and median of forty samples are depicted. P-values were calculated by comparing human proteins to *S. cerevisiae* proteins. *: $P < 0.05$; **: $P < 0.01$; ***: $P < 0.001$.

to display a 1.3-fold higher ER surface area compared to the control. However, those changes compared to the control were not significant ($P > 0.05$). To display the changes of the ER visually, we imaged the stained cells also by laser scanning confocal microscopy. The control cells presented the typical structure of the *S. cerevisiae* ER – they showed tubules extending from the perinuclear ER to the plasma membrane associated ER (Supplementary Fig. S3). The ER of the $\Delta\text{opi1}\Delta\text{rtn1}\Delta\text{rtn2}\Delta\text{yop1}$ quadruple deletion strain, appeared to display an increased area in comparison to the control strain. In comparison to the control strain the perinuclear ER of the quadruple deletion strain seemed extended and stained ER structures appeared to be increased (Supplementary Fig. S3). As a control, we evaluated the cell size by microscopy. All deletion strains showed a 1.4- to 1.5-fold larger cross-sectional cell area in comparison to the control ($P < 0.001$) with the quadruple deletion strain showing the greatest surface area in comparison to the control (Fig. 6b). The Δopi1 deletion strain, the $\Delta\text{opi1}\Delta\text{yop1}$ strain and the $\Delta\text{opi1}\Delta\text{rtn2}\Delta\text{yop1}$ triple deletion strain displayed a 1.4-fold cross-sectional cell area in comparison to the control whereas the $\Delta\text{opi1}\Delta\text{rtn1}\Delta\text{rtn2}\Delta\text{yop1}$ quadruple deletion strain showed a 1.5-fold cross-sectional cell area in comparison to the control. Thus, the deletion strains with expanded ER membrane area possess also a significantly increased cross-sectional cell area compared to the control strain.

3.4. Expansion of ER sheets diminished the induction of UPR

Physiologically, the UPR is induced in cells upon accumulation of unfolded proteins in the ER. However, also disruptions in the composition of the lipid bilayer membrane may activate the UPR (Shyu et al., 2019). To investigate differences in UPR induction, we integrated a GFP-based UPR-responsive reporter into the genome of selected deletion strains, Δopi1 , $\Delta\text{opi1}\Delta\text{yop1}$, $\Delta\text{opi1}\Delta\text{rtn2}\Delta\text{yop1}$, and $\Delta\text{opi1}\Delta\text{rtn1}\Delta\text{rtn2}\Delta\text{yop1}$, and two control strains, one without the IgG expression cassette and one expressing IgG. To calibrate the assay, we included three additional strains that were derived of the antibody expressing control, a Δire1 strain that cannot sense ER stress, and two strains with constitutively activated UPR expressing either *IRE1* or *HAC1*¹, respectively.

We performed a time-course experiment to identify the differences in the UPR response of the strains. Strains were first grown in non-inducing media, and at time point zero, the cultures were supplemented with 0.5% galactose to initialize the production of antibodies. Corresponding control cultures were supplemented with 0.5% glucose to repress the promoter. As expected, expression of either *IRE1* or *HAC1*¹ lead to activation of UPR in the absence of galactose and the response increased upon expression of the antibody. In contrast, the Δire1 strain was not

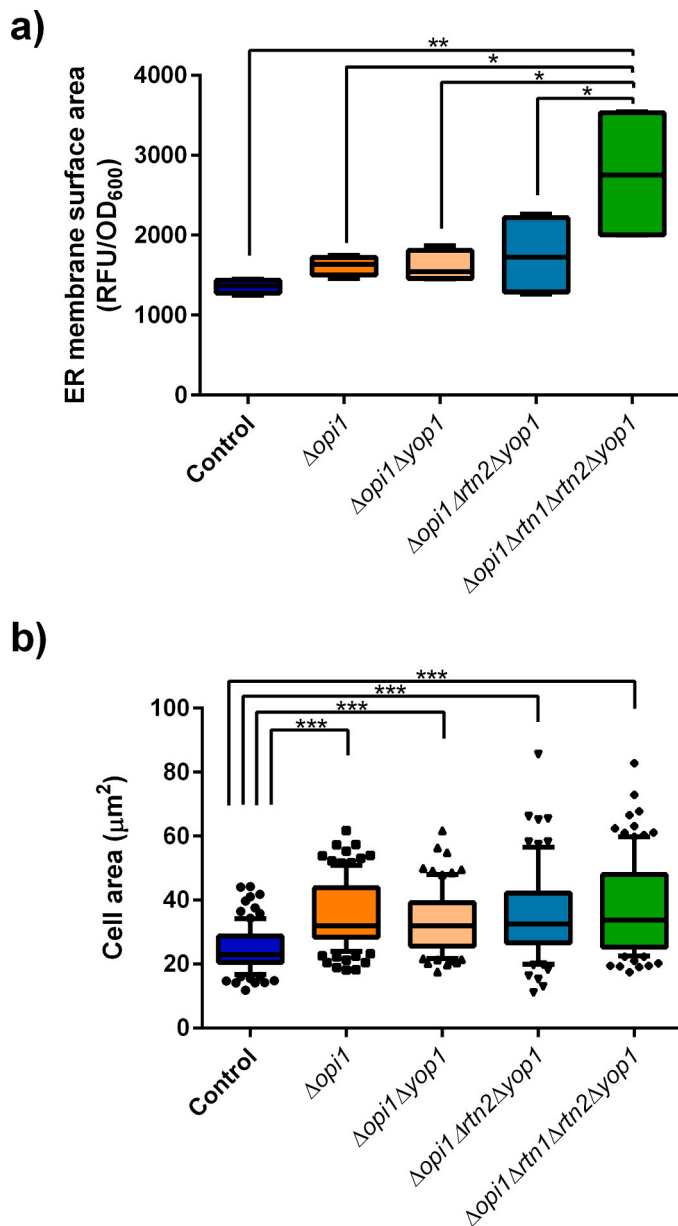


Fig. 6. The ER surface area and cross-sectional cell area are increased in deletion strains. The ER surface area and cell area of selected strains grown in 24-well deep well plates grown to early exponential phase was quantified. (a) ER surface area was quantified from cells stained with ER-Tracker™ Blue-White DPX. The OD₆₀₀ adjusted fluorescence signal (excitation 374 nm, emission 551 nm) expressed as RFU/OD₆₀₀ is depicted. The range, quartiles and median of four biological replicates are shown. P-values were calculated by pairwise comparison of all strains. Significant differences are marked. *: P < 0.05; **: P < 0.01; ***: P < 0.001. (b) The cross-sectional cell area was determined by microscopy analysis and expressed as μm². Between 72 and 107 yeast cells were evaluated per strain from five to seven different images. Cells were chosen randomly for analysis from cells residing in the same focal plane. The range, 10–90 percentile and median are shown. P-values were calculated by pairwise comparison of all strains. Significant differences are marked. *: P < 0.05; **: P < 0.01; ***: P < 0.001.

producing a significant UPR signal in the absence of galactose, but the strain exhibited a strong growth phenotype upon induction. In summary, these controls show that the reporter is activated by the cognate transcription factor Hac1^{1p} and can sense ER stress (Fig. 7a). The wild-type strain devoid of the antibody expression construct served as base line for UPR signal and addition of galactose did not produce a

noteworthy increase in the response. In contrast, the control strain expressing the IgG displayed a clear induction of UPR after induction of protein expression (Fig. 7a). Interestingly, all deletion strains displayed attenuated UPR compared to the control strain expressing IgG as evidenced by smaller or even absent GFP peaks and lower GFP reporter levels in the late exponential phase. The Δ*opi1*Δ*yop1* strain reached 83% of the control strains' maximal GFP reporter expression after 23 h of protein expression. The other deletion strains displayed even more attenuated UPR with maximal GFP values being 73% of the control strains' maximal GFP reporter expression (Fig. 7a). The variations observed in the timing of the maximal UPR induction (21–28 h) can most likely be accounted for by differences in the growth of the strains (Fig. 7b). Overall, these experiments show the importance of UPR for maintaining protein homeostasis and cellular fitness during antibody expression in cells with normal ER morphology and size. However, the reliance on UPR is diminished in cells with altered ER size and morphology.

4. Discussion

In this study we analyzed the effects of modifying the size and morphology of the ER of *S. cerevisiae* on its capacity for secretion of heterologous proteins. To this end, we created strains lacking the membrane curvature inducing genes (*RTN1*, *RTN2*, *YOP1*) alone or in combinations. As an additional variable, we created these strains in the presence or absence of Opi1p, one of the key regulators of lipid biosynthesis and thus on ER size.

In our work we observed that when expressing a full-length human antibody with these strains, the highest specific titers were produced by strains of the Opi1⁺ background. Among the strains of the Opi1⁺ background, the *OPI1* deletion itself had the most dominant effect on the productivity (Fig. 2a). However, our results indicate that deletion of membrane curvature inducing genes in addition to the *OPI1* gene is a viable approach to improve productivity further. We confirmed these results with a set of selected deletion strains that expressed another type of antibody molecule (Fig. 3a). The strains of the Opi1⁺ background that only possess deletions of membrane curvature inducing genes did not show a significant improvement in specific titers compared to the control, thus the expected increase in the sheet-to-tubule ratio did not seem to affect productivity. Thus, from these experiments we conclude that ER expansion is the more powerful approach to increase productivity compared to changing the ER sheet-to-tubule ratio. Furthermore, our current and earlier studies show that by ER expansion through depletion of Opi1p, the protein folding capacity of yeast cells can be increased benefitting mostly proteins of mammalian origin (SEAP, different antibodies, erythropoietin) but not endogenous proteins such as AP (de Ruijter et al., 2016b; Koskela et al., 2017, 2020). Furthermore, expression of AP was found to be titratable without reaching a saturating expression level (Koskela et al., 2020).

As also noted in earlier experiments with the *opi1* deletion strain (de Ruijter et al., 2016b; Koskela et al., 2017, 2020), all strains from the Opi1⁻ background exhibited a reduction in cell growth throughout all protein expression experiments. Although decreased cell growth is usually perceived as a challenge with protein producing strains, from an application point of view it is important to evaluate if the increased specific productivity would outweigh the reduced biomass production. However, as the focus in this work laid on testing a new cell engineering approach at small-scale, we cannot anticipate the effects of the strain modifications on protein production at larger scale.

We speculated that secreted mammalian proteins may benefit for folding from an increased ER lumen due to a higher content of hydrophobic amino acids and thus a higher propensity for aggregation. The analysis of the randomly sampled proteins showed that the median pI of the yeast proteins (5.23) is significantly lower than the median pI of the human proteins (7.42). The lower pI would indicate that the yeast polypeptides would be more strongly charged when present in the ER

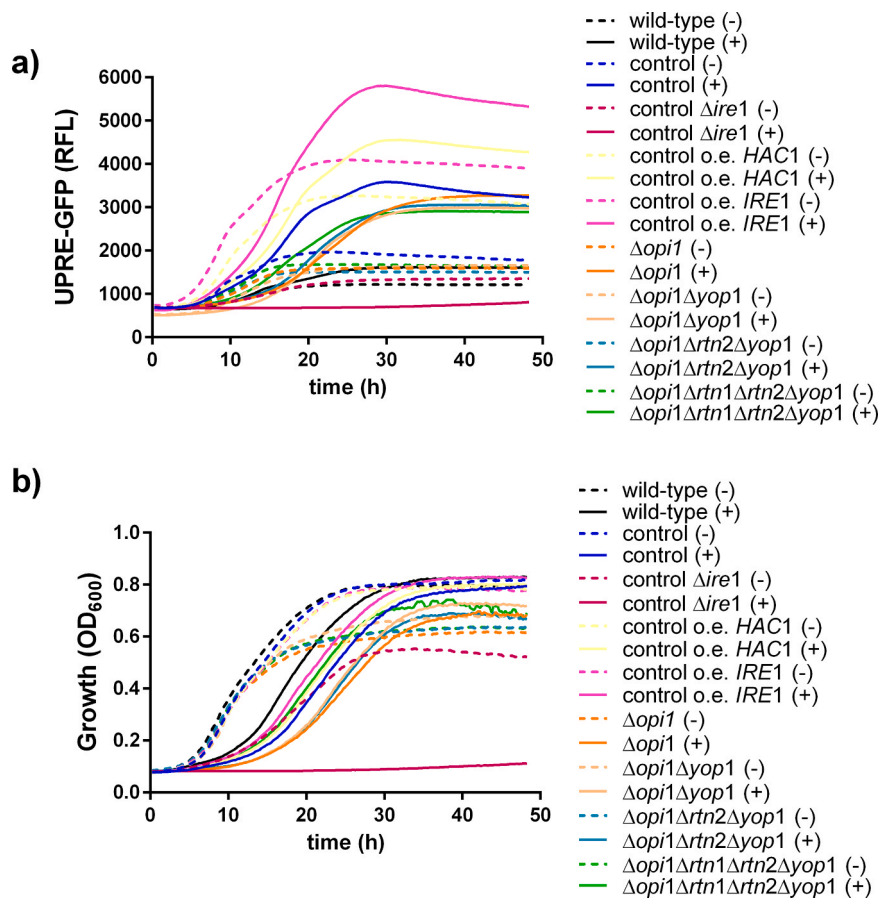


Fig. 7. UPR response is attenuated in strains with changed ER size and morphology. A GFP based genetic UPR sensor was integrated into selected antibody expressing deletion and control strains as well as into the wild-type strain. As controls served an antibody expressing strain (control), and the control strain with inactivated UPR sensing (*Δire1*) or constitutively active UPR (o.e. *HAC1*ⁱ or o.e. *IRE1*). Strains were grown in 96-well microtiter plates. Antibody expression was either induced with 0.5% galactose (continuous lines, + sign after strain name) or repressed with 0.5% glucose (dashed lines, - sign after strain name). UPR induction (GFP fluorescence) (a) and growth (b) were measured every 15 min for 48 h. Growth curves and GFP fluorescence represent averages from triplicate cultures.

providing a neutral pH environment (Fig. 5). Furthermore, the GRAVY of human proteins is significantly lower than the corresponding value of the yeast proteins. Overall, it is conceivable that the proteins of mammalian origin benefit more strongly from ER modifications due to their different physicochemical properties compared to their yeast counterparts.

The connection between the *OPI1* deletion and changes in the ER size and morphology has been detailed earlier revealing that the ER expansion occurred especially in the sheet area (Schuck et al., 2009a). Our experiments quantifying the ER surface area confirmed previous observations and in addition indicated that deletion of membrane curvature inducing genes led to further extensions of the ER membrane. The quadruple deletion strain contained a significantly higher ER surface area than the other deletion strains (Fig. 6a). However, the extent of the ER expansion did not correlate with the increased productivity (correlation coefficient < 0.2). Although we included a control experiment using *DGK1* overexpression that leads to perinuclear ER expansion, we cannot completely rule out that neither putative changes to the membrane lipid composition, due to the *OPI1* deletion, nor changes to the ER membrane curvature could affect either the membrane staining efficiency or the uptake of the staining reagent (Supplementary Fig. S2). However, the qualitative data from the confocal laser scanning microscopy further corroborates the quantitative data (Supplementary Fig. S3). Interestingly, we observed an accompanying increase in the cross-sectional area of the deletion strains. For this image analysis between 72 and 107 cells per strain were analyzed and the area of the mid-sections quantified (Fig. 6b). To our knowledge, there are no other

studies reporting a deregulated lipid synthesis, i.e. *OPI1* deletion, that coincides with increased cell dimensions.

A functional consequence of the deletions of *RTN1*, *RTN2*, *YOP1*, and *OPI1* was the generation of yeast strains that displayed an attenuated UPR under protein expressing conditions (Fig. 6). However, UPR induction is a two-sided sword; on one hand it increases expression of 300 genes in yeast that represents a substantial cellular burden (Travers et al., 2000), on the other hand, its activation has been shown to improve productivity (Valkonen et al., 2003). Thus, an attenuated induction of UPR might be ideal, benefitting from an optimized secretory pathway, but at reduced costs for the cells. ER expansion was shown earlier to alleviate UPR, and it was suggested that the expanded ER could either promote protein folding or tolerance for misfolded proteins in the ER (Schuck et al., 2009a). Alternatively, the absence of Rtn1p, Rtn2p, Yop1p and Opi1p or the expansion of sheets could affect the localization or the local concentrations of the UPR-sensor Ire1p, preventing its dimerization and activation (Kimata et al., 2007). Furthermore, localization of membrane proteins can be affected by lipid rafts, which are segregated functional units within membranes, and these rafts have been implicated to be present in the yeast ER and participate in protein secretion (Bagnat et al., 2000; Helms and Zurzolo, 2004). The membrane-interacting proteins Rtn1p, Rtn2p, and Yop1p could participate in the formation of Ire1p containing rafts that act as areas of UPR control. In this case, the absence of the proteins could cause Ire1p to disperse throughout the ER making the local concentrations too low to initiate dimerization and subsequent activation.

While we interpreted our results that the expanded ER would

promote folding, also alternative mechanisms improving expression cannot be disregarded. It is possible that the proliferation of sheets creates additional space for high-density ribosome binding and translocation (West et al., 2011), aiding the entrance of the heavy and light chain polypeptides to the ER and secretory pathway. Furthermore, expansion of sheets can also affect the dynamics of ER exit sites (ERES), which localize to the high-curvature areas. ERES have been shown to accumulate to fewer distinct sites in $\Delta rtn1\Delta rtn2\Delta yop1$ triple deletion strains as these strains displayed fewer tubules and fewer high-curvature areas than the parental strain (Okamoto et al., 2012). It is notable that this ERES organization is more similar to the ERES structures in the protein producer *Pichia pastoris* (Kurokawa and Nakano, 2019).

We observed also growth defects for two of the deletion strains. When grown under non-inducing conditions, the spotting assays revealed only minor growth defects. Surprisingly, $\Delta rtn1$ and $\Delta rtn1\Delta rtn2\Delta yop1$ strains did not grow under inducing conditions neither on solid medium nor in liquid medium (Figs. 1b, 2b). The two strains exhibited a very long lag-phase when grown in the presence of galactose. When these deletions were combined with $\Delta opi1$, these defects were absent. There are several putative causes for the reduced growth of the deletion strains. It was reported that the $\Delta rtn1\Delta rtn2\Delta yop1$ deletion strain shows altered ER inheritance which might lead to a growth defect (Chao et al., 2021; Pina et al., 2016). The growth defects only materialized in presence of the UPR inducing reagent tunicamycin. Moreover, when all ER membrane curvature inducing genes were deleted, these modifications caused aberrations in lipid droplet formation and other functions related to lipid biosynthesis. It has been noticed that these changes may lead to accumulations of PA to toxic levels (Ganesan et al., 2020).

Overall, our study explored the contribution of ER morphology and size on recombinant protein production, and we could reveal that cellular productivity can benefit from an altered ER morphology, however, only when the ER membrane area is expanded. A functional consequence of the ER modifications was an attenuated UPR in the engineered strains that could be a contributing factor in enhancing cellular productivity in addition to the extended ER membrane area. Importantly, the reticulon proteins are highly conserved and found in many eukaryotic organisms of biotechnological interest. Thus, it might be valuable to evaluate the strategy of modifying the ER morphology for recombinant protein production also in other fungal organisms such as *Komagataella pastoris*, *Trichoderma reesei*, or *Aspergillus niger*, although those proteins remain to be characterized first. From a more general perspective, our study highlights the potential that engineering of sub-cellular structures can have on increasing cellular productivity.

CRediT authorship contribution statement

Alexander Daniel Frey: Writing – review & editing, Writing – original draft, Supervision, Investigation, Conceptualization. **Essi V. Koskela:** Writing – review & editing, Investigation, Conceptualization. **Laura R. K. Niemelä:** Writing – review & editing, Methodology, Investigation, Formal analysis.

Declaration of Competing Interest

The authors declare that they have no known competing financial interests or personal relationships that could have appeared to influence the work reported in this paper.

Data availability

Data will be made available on request.

Appendix A. Supporting information

Supplementary data associated with this article can be found in the online version at [doi:10.1016/j.jbiotec.2024.03.009](https://doi.org/10.1016/j.jbiotec.2024.03.009).

References

- Bagnat, M., Keränen, S., Shevchenko, A., Shevchenko, A., Simons, K., 2000. Lipid rafts function in biosynthetic delivery of proteins to the cell surface in yeast. *Proc. Natl. Acad. Sci. USA* 97, 3254–3259. <https://doi.org/10.1073/pnas.97.7.3254>.
- Bao, J., Huang, M., Petranovic, D., Nielsen, J., 2018. Balanced trafficking between the ER and the Golgi apparatus increases protein secretion in yeast. *AMB Express* 8, 37. <https://doi.org/10.1186/s13568-018-0571-x>.
- Chao, J.T., Pina, F., Niwa, M., 2021. Regulation of the early stages of endoplasmic reticulum inheritance during ER stress. *Mol. Biol. Cell* 32, 109–119. <https://doi.org/10.1091/mbc.E20-08-0558>.
- Chen, S., Novick, P., Ferro-Novick, S., 2012. ER network formation requires a balance of the dynamin-like GTPase Sey1p and the Lunapark family member Lnp1p. *Nat. Cell Biol.* 14, 707–716. <https://doi.org/10.1038/ncb2523>.
- Davy, A.M., Kildegaard, H.F., Andersen, M.R., 2017. Cell factory engineering. *Cell Syst.* 4, 262–275. <https://doi.org/10.1016/j.cels.2017.02.010>.
- Diwu, Z., Zhang, C., Klauert, D.H., Haugland, R.P., 2000. Fluorescent molecular probes VI The spectral properties and potential biological applications of water-soluble Dapoxyl TM sulfonic acid, *Journal of Photochemistry and Photobiology A: Chemistry*.
- Ganesan, S., Tavassoli, M., Shabits, B.N., Zarembeg, V., 2020. Tubular ER associates with diacylglycerol-rich structures during lipid droplet consumption. *Front. Cell Dev. Biol.* 8, 1–17. <https://doi.org/10.3389/fcell.2020.00700>.
- Gietz, R., Schiestl, R., 2007. Large-scale high-efficiency yeast transformation using the LiAc/SS carrier DNA/PEG method. *Nat. Protoc.* 2, 38–41.
- Guerfal, M., Claes, K., Knittelfelder, O., Rycke, R.De, Kohlwein, S.D., Callewaert, N., De Rycke, R., Kohlwein, S.D., Callewaert, N., 2013. Enhanced membrane protein expression by engineering increased intracellular membrane production. *Microb. Cell Fact.* 12, 122. <https://doi.org/10.1186/1475-2859-12-122>.
- Hammer, S.K., Avalos, J.L., 2017. Harnessing yeast organelles for metabolic engineering. *Nat. Chem. Biol.* 13, 823–832. <https://doi.org/10.1038/nchembio.2429>.
- Han, G.-S., O'Hara, L., Carman, G.M., Siniouoglou, S., 2008. An unconventional diacylglycerol kinase that regulates phospholipid synthesis and nuclear membrane growth. *J. Biol. Chem.* 283, 20433–20442. <https://doi.org/10.1074/jbc.M802903200>.
- Hegemann, J.H., Heick, S.B., 2011. Delete and repeat: a comprehensive toolkit for sequential gene knockout in the budding yeast *Saccharomyces cerevisiae*. *Methods Mol. Biol.* (Clifton, N. J.) 189–206. https://doi.org/10.1007/978-1-61779-197-0_12.
- Helms, J.B., Zurzolo, C., 2004. Lipids as targeting signals: lipid rafts and intracellular trafficking. *Traffic* 5, 247–254. <https://doi.org/10.1111/j.1600-0854.2004.0181.x>.
- Kimata, Y., Ishiwata-Kimata, Y., Ito, T., Hirata, A., Suzuki, T., Oikawa, D., Takeuchi, M., Kohno, K., 2007. Two regulatory steps of ER-stress sensor Ire1 involving its cluster formation and interaction with unfolded proteins. *J. Cell Biol.* 179, 75–86. <https://doi.org/10.1083/jcb.200704166>.
- Koskela, E.V., de Ruijter, J.C., Frey, A.D., 2017. Following nature's roadmap: folding factors from plasma cells led to improvements in antibody secretion in *S. cerevisiae*. *Biotechnol. J.* 12, 1–13. <https://doi.org/10.1002/biot.201600631>.
- Koskela, E.V., Gonzalez Salcedo, A., Piirainen, M.A., Iivonen, H.A., Salminen, H., Frey, A.D., 2020. Mining data from plasma cell differentiation identified novel genes for engineering of a yeast antibody factory. *Front. Bioeng. Biotechnol.* 8, 1–16. <https://doi.org/10.3389/fbioe.2020.00255>.
- Kurokawa, K., Nakano, A., 2019. The ER exit sites are specialized ER zones for the transport of cargo proteins from the ER to the Golgi apparatus. *J. Biochem.* 165 (2), 109–114. <https://doi.org/10.1093/jb/mvy080>.
- Kyte, J., Doolittle, R.F., 1982. A simple method for displaying the hydropathic character of a protein. *J. Mol. Biol.* 157, 105–132. [https://doi.org/10.1016/0022-2836\(82\)90515-0](https://doi.org/10.1016/0022-2836(82)90515-0).
- Love, K.R., Politano, T.J., Panagiotou, V., Jiang, B., Stadheim, T.A., Love, J.C., 2012. Systematic single-cell analysis of *Pichia pastoris* reveals secretory capacity limits productivity. *PLoS One* 7, e37915. <https://doi.org/10.1371/journal.pone.0037915>.
- Okamoto, M., Kurokawa, K., Matsuura-Tokita, K., Saito, C., Hirata, R., Nakano, A., 2012. High-curvature domains of the ER are important for the organization of ER exit sites in *Saccharomyces cerevisiae*. *J. Cell Sci.* 125, 3412–3420. <https://doi.org/10.1242/jcs.100065>.
- Parsaie Nasab, F., Aebi, M., Bernhard, G., Frey, A.D., 2013. A combined system for engineering glycosylation efficiency and glycan structure in *Saccharomyces cerevisiae*. *Appl. Environ. Microbiol.* 79, 997–1007. <https://doi.org/10.1128/AEM.02817-12>.
- Piirainen, M.A., Frey, A.D., 2020. Investigating the role of ERAD on antibody processing in glycoengineered *Saccharomyces cerevisiae*. *FEMS Yeast Res.* 20, 1–11. <https://doi.org/10.1093/femsyr/foaa002>.
- Pina, F.J., Fleming, T., Pogliano, K., Niwa, M., 2016. Reticulons regulate the ER inheritance block during ER stress. *Dev. Cell* 37, 279–288. <https://doi.org/10.1016/j.devcel.2016.03.025>.
- Pincus, D., Chevalier, M.W., Aragón, T., van Anken, E., Vidal, S.E., El-Samad, H., Walter, P., 2010. BiP binding to the ER-stress sensor Ire1 tunes the homeostatic behavior of the unfolded protein response. *PLoS Biol.* 8 <https://doi.org/10.1371/journal.pbio.1000415>.
- de Ruijter, J.C., Frey, A.D., 2015. Analysis of antibody production in *Saccharomyces cerevisiae*: effects of ER protein quality control disruption. *Appl. Microbiol. Biotechnol.* 99, 9061–9071. <https://doi.org/10.1007/s00253-015-6807-7>.
- de Ruijter, J.C., Jurgens, G., Frey, A.D., 2016a. Screening for novel genes of *Saccharomyces cerevisiae* involved in recombinant antibody production. *FEMS Yeast Res.* 17 (1), 10. <https://doi.org/10.1093/femsyr/fow104>.

- de Ruijter, J.C., Koskela, E.V., Frey, A.D., 2016b. Enhancing antibody folding and secretion by tailoring the *Saccharomyces cerevisiae* endoplasmic reticulum. *Micro Cell Fact.* 15, 87. <https://doi.org/10.1186/s12934-016-0488-5>.
- Schuck, S., Prinz, W.A., Thorn, K.S., Voss, C., Walter, P., 2009b. Membrane expansion alleviates endoplasmic reticulum stress independently of the unfolded protein response. *J. Cell Biol.* 187, 525–536. <https://doi.org/10.1083/jcb.200907074>.
- Schuck, S., Prinz, W.A., Thorn, K.S., Voss, C., Walter, P., 2009a. Membrane expansion alleviates endoplasmic reticulum stress independently of the unfolded protein response. *J. Cell Biol.* 187, 525–536. <https://doi.org/10.1083/jcb.200907074>.
- Shibata, Y., Shemesh, T., Prinz, W.A., Palazzo, A.F., Kozlov, M.M., Rapoport, T.A., 2010. Mechanisms determining the morphology of the peripheral ER. *Cell* 143, 774–788. <https://doi.org/10.1016/j.cell.2010.11.007>.
- Shusta, E.V., Raines, R.T., Plückthun, A., Wittrup, K.D., Plückthun, A., Wittrup, K.D., 1998. Increasing the secretory capacity of *Saccharomyces cerevisiae* for production of single-chain antibody fragments. *Nat. Biotechnol.* 16, 773–777. <https://doi.org/10.1038/nbt0898-773>.
- Shyu, P., Ng, B.S.H., Ho, N., Chaw, R., Seah, Y.L., Marvalim, C., Thibault, G., 2019. Membrane phospholipid alteration causes chronic ER stress through early degradation of homeostatic ER-resident proteins. *Sci. Rep.* 9, 8637. <https://doi.org/10.1038/s41598-019-45020-6>.
- Travers, K.J., Patil, C.K., Wodicka, L., Lockhart, D.J., Weissman, J.S., Walter, P., 2000. Functional and genomic analyses reveal an essential coordination between the unfolded protein response and ER-associated degradation. *Cell* 101, 249–258. [https://doi.org/S0092-8674\(00\)80835-1](https://doi.org/S0092-8674(00)80835-1) [pii].
- Valkonen, M., Penttilä, M., Saloheimo, M., 2003. Effects of inactivation and constitutive expression of the unfolded-protein response pathway on protein production in the yeast *Saccharomyces cerevisiae*. *Appl. Environ. Microbiol.* 69, 2065–2072. <https://doi.org/10.1128/AEM.69.4.2065>.
- Voeltz, G.K., Prinz, W.A., Shibata, Y., Rist, J.M., Rapoport, T.A., 2006. A class of membrane proteins shaping the tubular endoplasmic reticulum. *Cell* 124, 573–586. <https://doi.org/10.1016/j.cell.2005.11.047>.
- Walter, J.D., Scherer, M., Hutter, C.A.J., Garaeva, A.A., Zimmermann, I., Wyss, M., Rheinberger, J., Ruedin, Y., Earp, J.C., Egloff, P., Sorgenfrei, M., Hürlimann, L.M., Gonda, I., Meier, G., Remm, S., Thavarasah, S., van Geest, G., Bruggmann, R., Zimmer, G., Slotboom, D.J., Paulino, C., Plattet, P., Seeger, M.A., 2022. Biparatopic sybodies neutralize SARS-CoV-2 variants of concern and mitigate drug resistance. *EMBO Rep.* 23. <https://doi.org/10.15252/embr.202154199>.
- West, M., Zurek, N., Hoenger, A., Voeltz, G.K., 2011. A 3D analysis of yeast ER structure reveals how ER domains are organized by membrane curvature. *J. Cell Biol.* 193, 333–346. <https://doi.org/10.1083/jcb.201011039>.
- Westrate, L.M., Lee, J.E., Prinz, W.A., Voeltz, G.K., 2015. Form follows function: the importance of endoplasmic reticulum shape. *Annu Rev. Biochem.* 84, 791–811. <https://doi.org/10.1146/annurev-biochem-072711-163501>.